This document is a non-peer reviewed preprint submitted to EarthArXiv

The Overlooked Sub-Grid Air-Sea Flux in Climate Models

Julius J.M. Busecke[†*1], Dhruv Balwada[†1], Paige E. Martin[1], Thomas E.G. Nicholas[1], Zoe C.P. Johnson[3], Charles I. Stern[1], and Ryan P. Abernathey[1]

[1]Lamont Doherty Earth Observatory, Columbia University, Palisades, NY, USA
[2]Barnard College of Columbia University, New York, NY, USA

Abstract

Understanding air-sea interaction is crucial for our ability to predict future states of the climate system, and to inform economic and societal decision-making[9;8]. However, the representation of air-sea interactions in climate models is limited by structural errors associated with model resolution[15;24;31]. Coarse-resolution climate models do not resolve small-scale structures in the air-sea state, which, due to strong nonlinearities in the coupling formulae, can impact the large-scale air-sea exchange—a mechanism that has received little attention and is the focus of this paper. Since observations at the temporal and spatial coverage needed to study this problem do not yet exist, we quantify the impact of this small-scale heterogeneity on the large-scale air-sea heat flux by analyzing $1/10°$ coupled climate simulations. This effect systematically cools the ocean by about $4W/m^2$ globally—with large spatio-temporal variations—and mostly enhances the large-scale heat flux. By identifying an overlooked contribution to air-sea heat flux in climate models, we open a promising new direction for addressing biases in climate simulations and thus improving future climate predictions. Furthermore, future observations, like the newly proposed satellite mission ODYSEA[35], could potentially observe and quantify this effect directly.

1 Introduction

The air-sea exchange of heat plays a fundamental role in the dynamics of the atmosphere and ocean and, consequently, in the evolution of Earth's weather and climate. This exchange impacts processes across a wide spectrum of spatial and temporal scales; ranging from short-term (e.g. the rapid modulation of boundary layer turbulence or impacts on hurricane generation and evolution) to longer-term (e.g. the evolution of the El-Niño Southern Oscillation)[9]. Air-sea heat flux also plays a central role in the trajectory of global climate; the ocean has absorbed about 90% of the excess heat due to anthropogenic climate change, leading to unprecedented ocean warming[17].

Accurately representing the air-sea heat flux is essential for developing reliable coupled climate models, our primary tool for understanding past and future changes in Earth's climate[8]. The current generation of coarse-resolution (1^o or coarser) climate models, which make up the large majority of the Coupled Model Intercomparison Project (CMIP)[10], exhibit global and regional biases in sea surface

[†]These authors contributed equally to this work.
[*]Corresponding author: julius@ldeo.columbia.edu

temperature (SST) and its trends, raising concerns about the predictive skill of these models[25;39]. Among other factors, structural errors associated with model resolution[15;24] and air-sea coupling[31;5] have been identified as some of the key sources of uncertainity and bias.

There is a rich and rapidly growing literature (recent comprehensive reviews can be found in[29;26]) that demonstrates the impacts of small-scale (mesoscale and sub-mesoscale) oceanic variability and high-frequency atmospheric variability on processes that are active at the air-sea interface and in the associated boundary layers, a region sometimes collectively referred to as the air-sea transition zone[8]. These small-scale flows modulate the structure and circulation of the atmospheric boundary layer, which feeds back onto the buoyancy (heat and freshwater) and mechanical (momentum) fluxes. On the ocean side, even a homogeneous atmospheric flow over a heterogeneous ocean covered with fronts and filaments leads to a highly variable response in the wind stress, air-sea heat fluxes, and upper ocean turbulence. High-frequency atmospheric variability, e.g. gustiness and storms, is also crucial in impacting the upper ocean boundary layers, entrainment, and air-sea fluxes of buoyancy and gases. All this variability also results in rectified impacts on upper ocean stratification and the kinetic and potential energy reservoirs[21;3]. Furthermore, these coupled effects may impact atmospheric storm track structures, western boundary current variability, and eventually large-scale atmosphere and ocean circulations.

Many of these insights into the small-scale coupling mechanisms and their impacts on larger scales have come from process-based analysis of high-resolution coupled simulations[33], comparison of coupled models across resolutions[28], or by running experiments that modify the scale of coupling by filtering the input fields that are passed into the coupler[36]. While these efforts are essential for furthering our understanding of air-sea interactions and their impacts, development of parameterizations is essential to ensure that the impacts of these small-scale processes can be properly accounted for in coarse-resolution simulations. Parameterizations accounting for many missing processes, such as radiation, cloud microphysics, moist convection, momentum and buoyancy transport by sub-mesoscale and mesoscale eddies, turbulent mixing in boundary layers, and wave breaking, are already an essential ingredient in atmospheric and oceanic models[7]. While, parameterizations accounting for impact of temporal atmospheric wind variability —gustiness—on the air-sea flux have been developed[12;4;2], no parameterizations comprehensively account for all the different components of spatial heterogeneity at the air-sea interface. Heterogeneity is not purely a challenge at the interface of the ocean and atmosphere; complementary progress is also being made in implementing parameterizations for land-atmosphere heterogeneity in climate models[11].

Turbulent fluxes across the air-sea interface are parameterized with the help of bulk formulae, semi-empirical equations which are calibrated with the help of station-based observations of eddy-correlation fluxes[9]. Due to the localized nature of these observations, the bulk formulae are not necessarily representative of turbulent fluxes over entire model grid boxes. These model grid boxes represent large areas compared to the localized observations, and thus a methodology to account for net rectified impacts of sub-grid scale heterogeneity needs to be developed. While the net impact of this heterogeneity is not accounted for, it has been shown that accounting for the variability due to sub-grid flows using stochastic approaches may be important[37;20]. Gustiness parameterizations account for unresolved atmospheric mesoscale *temporal* variability of atmospheric winds[4;2], but no comparable parameterization accounts for sub-grid *spatial* heterogeneity generated by atmospheric and oceanic flows.

A comprehensive assessment of this missing sub-grid air-sea heat flux due to spatial heterogeneity is absent from the literature. This might partially be due to a dearth of direct high *spatial* resolution observations of the coupled air-sea state. While still no direct, long-term, high-resolution global observations of the coupled air-sea state exist, the latest generation of high-resolution coupled climate models represent a much wider range of atmospheric and oceanic motions than their low-resolution counterparts. These model also generally show a tendency towards reduced biases[13]. Our study uses state-of-the-art high-resolution coupled climate simulations to show that the impact of small-scale heterogeneity, missing from most climate simulations, can be large and should be parameterized.

2 Accounting for the impact of sub-grid heterogeneity on turbulent air-sea heat flux

We quantify the impact of small-scale heterogeneity on the turbulent air-sea heat fluxes with the help of spatial filtering and computing heat fluxes offline (details provided in Methods section). Spatial filtering is used to construct low-resolution surrogate–surface fields that are comparable in spatio-temporal variability to most low-resolution climate simulation–from a high-resolution simulation. The small-scale turbulent heat flux (Q^*) is calculated as the difference between the net impact of the high-resolution flux on large-scales and the flux that could be computed if only the large-scale flow fields were known,

$$Q^* = \overline{Q} - \overline{Q^c}, \tag{1}$$

where Q is the flux computed using the high-resolution fields, Q^c is the flux computed using the low-resolution surrogate (filtered) fields, and $\overline{(.)}$ denotes the spatial filtering operator. Note that Q^* is not the full small-scale spatial variability in the heat flux ($Q - Q^c$), but rather the net impact of this on the large-scale that would be missing in a model with no small-scale heterogeneity. If needed, the small-scale spatial variability in $Q - Q^c$ could be quantified using higher moments of the distribution (e.g. standard deviation), but this is not the focus of our study. As explained in the Methods section, these computations are carried out separately for the sensible and latent turbulent heat fluxes, but for brevity we only discuss the total turbulent heat flux (latent + sensible) throughout the main text. This methodology is visually summarized in Figure 1. (Results for individual components and daily examples of each component can be found in the Supplementary Material).

3 Results

3.1 Patterns of small-scale air-sea turbulent heat flux

The small-scale air-sea flux (Q^*) shows strong spatial and temporal variability, locally reaching values up to O(100) W/m^2 (Figure 3 and Supplementary Material Figure 2). The long time (20 year) mean of Q^* (Figure 2b) indicates that the small-scales mostly cool the ocean, enhancing the large-scale fluxes (Figure 2a). Some of the most prominent deviations from this cooling pattern, warming of the ocean, arise near the equator and in the more energetic parts of the Antarctic Circumpolar Current (ACC). The strongest time-mean heat loss, exceeding 20 W/m^2, is seen in highly energetic parts of the ocean, such as the western boundary currents and the Agulhas retroflection. Away from these regions of strong heat loss, the time-mean Q^* reaches values of O(1) W/m^2 over much of the open ocean. A global area-weighted average of this time-mean Q^* corresponds to a heat loss of $\sim$4 W/m^2 (Figure 2b). For comparison, Earth's energy imbalance at the top of the atmosphere is currently warming our planet at a rate of $\sim 1W/m^2$, and about 90% of this excess heat is ending up in the ocean[18;17].

As discussed above, in most regions of the ocean the time-mean Q^* has the same sign as, and thus enhances, the time-mean large-scale flux ($\overline{Q^c}$). This enhancement is not only limited in the time-mean,

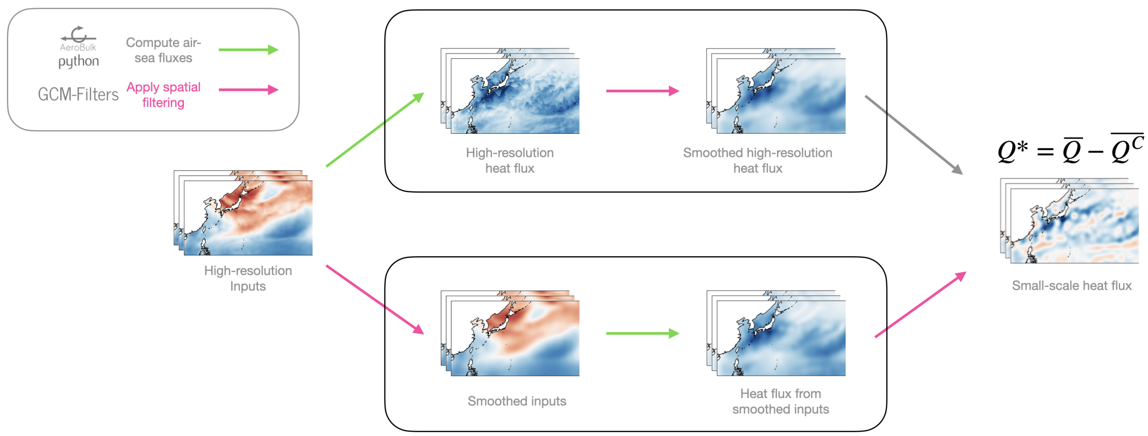

Figure 1: Methodology for separating contributions of large and small scales to air-sea flux. Starting with high-resolution ocean and atmosphere fields on the left we apply two main operations: offline computation of turbulent heat fluxes (green arrows), and spatial filtering (magenta arrows) to separate small-scale structures in different order. The upper path illustrates the method to compute $\overline{Q}$ and the lower path illustrates $\overline{Q^C}$. See Methods for details.

and even daily average values of Q^* predominantly enhance $\overline{Q_c}$ (Figure 3). Around 70% of the daily average values have Q^* enhancing $\overline{Q_c}$ (same sign), and over 20% of the values show an enhancement exceeding 10% of the magnitude of $\overline{Q_c}$. Within the western boundary current regions this enhancement is even more pronounced (with 77% of all values acting to enhance, and 35% exceeding 10% of the large-scale flux; see text inset in Figure 3 and gray boxes in Figure 2 for reference). These strong local enhancement events could be vital for improving the representation of extreme events, like marine heatwaves[23] and atmospheric rivers[34] in coarse resolution models.

3.2 Oceanic vs atmospheric contributions to small-scale air-sea turbulent heat flux

Is it the small-scale heterogeneity of the ocean or the atmosphere that is driving the patterns of Q^*? To separate the degree to which atmospheric versus oceanic small-scale features contribute to Q^*, we consider two cases where the input variables from only the atmosphere or the ocean are filtered. The contribution coming from small-scale heterogeneity in the atmosphere is denoted $Q^{*,A}$, where only the atmopsheric input fields are filtered when computing the large-scale flux (Q^c). The oceanic counterpart is denoted by $Q^{*,O}$, where only the oceanic input fields are filtered. Here we discuss the results primarily in terms of the long-time (20-year) average of these terms (Figure 4). Further details of these computations can be found in the Methods section.

The contribution to the sub-grid flux (Q^*) due to small-scale atmospheric features ($Q^{*,A}$) produces a spatially smooth cooling effect over much of the ocean. Hot spots in $Q^{*,A}$ emerge in a few regions that have cold wind bursts off continents, such as east of the North American continent in the western Atlantic Ocean. In contrast, the contribution from small-scale oceanic features ($Q^{*,O}$) is highly spatially variable and results in both warming and cooling of the ocean. As expected, dynamically active

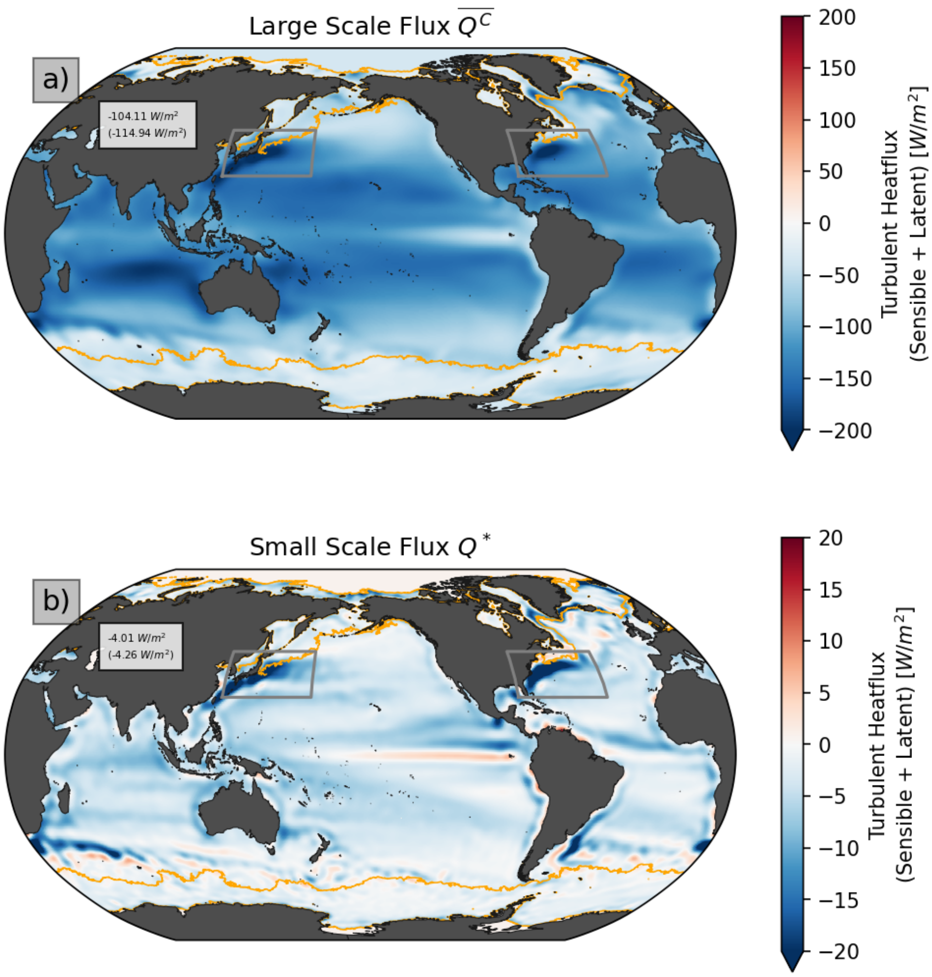

Figure 2: 20-year time averaged results for the CM2.6 simulation. **a)** shows the large scale flux $\overline{Q^C}$ and **b)** shows the small scale flux Q^* (for details see Equation 1). Negative values indicate ocean heat loss. Grey boxes indicate the western boundary current regions used in Figure 3. Orange lines indicate the maximum extent of sea ice. Numbers shown in the top left of map panels indicate globally averaged values for all available values and for only ice free locations in parentheses. For details on treatment of sea ice and temporal averaging see Supplementary Materials.

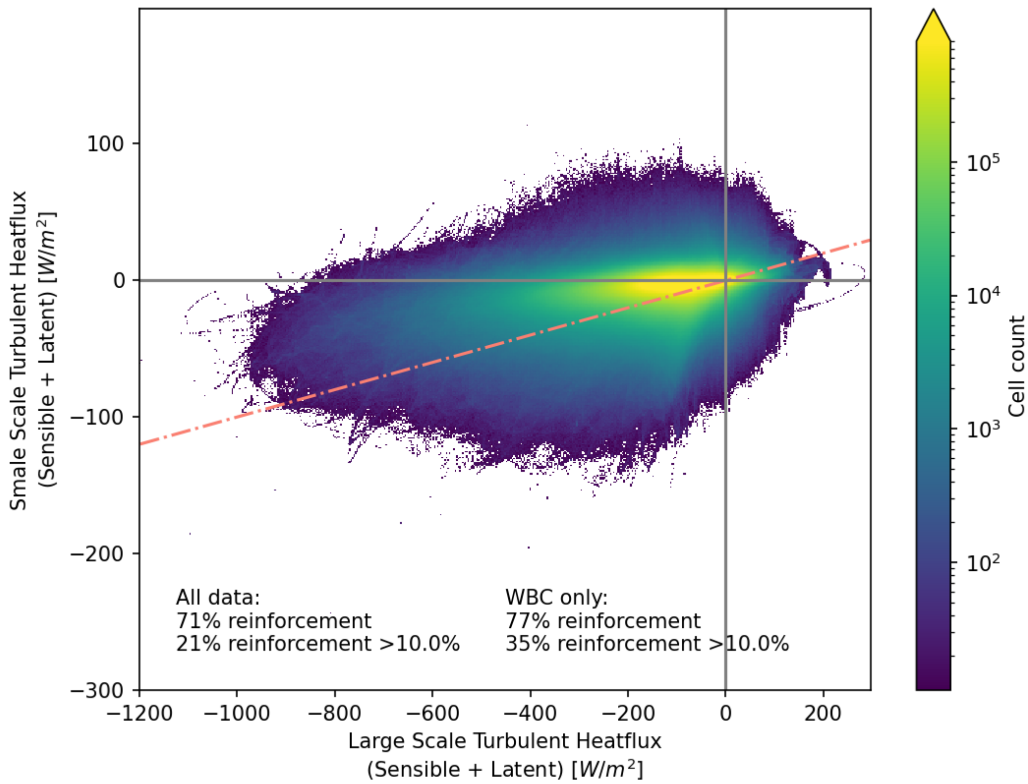

Figure 3: Bivariate histogram showing the relationship between the large-scale flux $\overline{Q^C}$ on the x-axis and the small scale flux Q^* on the y-axis for 1 year of the CM2.6 simulation. Points falling in the upper-right and lower-left quadrants indicate that the small scale flux is the same sign as and enhancing the large scale flux. Points falling below the red dashed line in the lower-left quadrant and above the red dashed line in the upper-right quadrant are enhancing the large-scale flux by more than 10%. The percentage of datapoints for the full domain ('All data') and just the western boundary current ('WBC only'; gray boxes in Figure 2) categorized as enhancing and enhancing more than 10% are shown at the lower left. Note that the interannual variability of Q^* is small (see Supplementary Material) and thus this relationship is representative of the full-time frame.

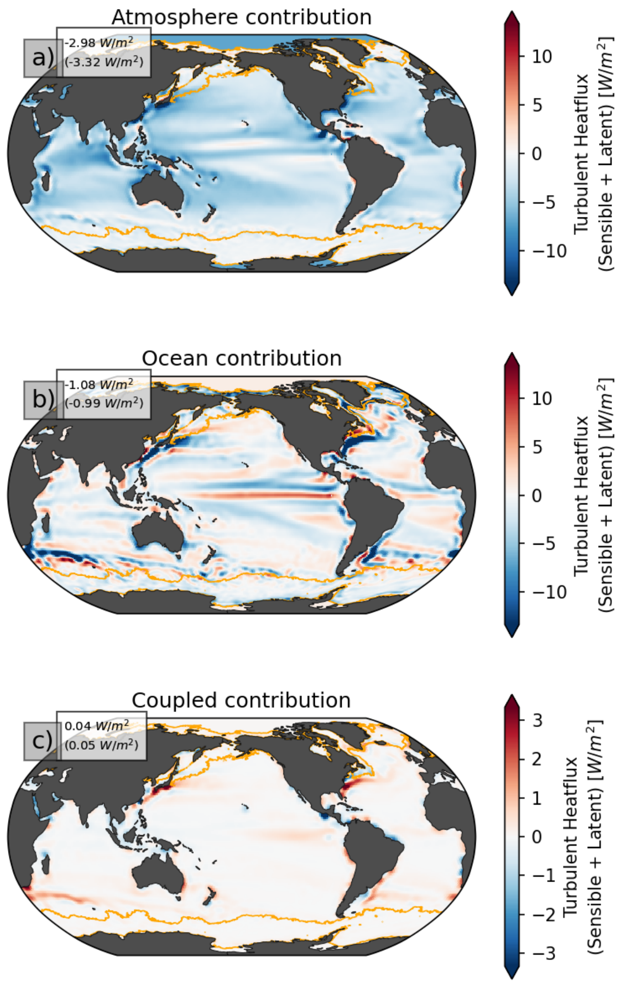

Figure 4: 20-year time-average decomposed small-scale flux Q^* for the CM2.6 simulation. **a)** shows the contribution only from the atmospheric fields $Q^{*,A}$, **b)** shows the contribution only from the oceanic fields $Q^{*,O}$, and **c)** shows the coupled contribution $Q^{*,O-A}$, resulting from the interplay of small scales in both ocean and atmosphere and defined as the residual (See Methods section 5.4). Negative values indicate heat flux from the ocean to the atmosphere. Orange lines indicate the maximum extent of sea ice. Numbers shown in the top left of map panels indicate globally averaged values for all available values and for only ice free locations in parentheses. For details on treatment of sea ice and temporal averaging see Supplementary Materials.

regions with large oceanic variability contribute most strongly to $Q^{*,O}$. The global area average of $Q^{*,A}$ and $Q^{*,O}$ correspond to a cooling of 3 W/m^2 and 1 W/m^2 respectively, with $Q^{*,A}$ corresponding to about 75% of the globally averaged small-scale heat loss (Q^*) of 4 W/m^2. However, locally $Q^{*,O}$ can be much larger than $Q^{*,A}$ and potentially play a leading role in the regional dynamics.

The contribution to the sub-grid flux coming from the coupled small-scale flow heterogeneity is denoted as $Q^{*,O-A}$, and computed as a residual (see methods section). $Q^{*,O-A}$ is found to be one or two orders of magnitude smaller than $Q^{*,A}$ and $Q^{*,O}$ (Figure 4c), often $Q^{*,O-A}$ is opposite signed to $Q^{*,O}$. This smallness of $Q^{*,O-A}$ may be expected, as the spatio-temporal scales of oceanic (slow and small) and atmospheric flows (fast and large) are very different, and the correlation between the two may be expected to be a sub-dominant contributor to the flux arising from small-scale heterogeneity. Much of the small-scale heterogeneity at the air-sea interface arises due to the internal variability resulting from the disparate instabilities of the individual fluids, rather than due to coupled interactions.

To further understand the role of the atmosphere and the ocean, we also conducted a second decomposition where we filtered either the velocity fields or the tracer fields when computing fluxes. This allows us to evaluate the contribution coming from the small-scale heterogeneity in these particular flow variables, which can be contrasted to the above decomposition into fluids (see Supplementary Material for figures). This analysis showed that $Q^{*,A}$ gets almost all of its contribution from the velocity fields (primarily wind heterogeneity), and $Q^{*,O}$ gets almost all of its contribution from the tracer fields (primarily sea surface temperature - SST - heterogeneity). While gustiness parameterizations address the missing impact of unresolved temporal atmospheric wind variability, which may be similar to the atmospheric spatial sub-grid wind heterogeneity, our study is the first to estimate and contrast the impact of sub-grid oceanic surface temperature heterogeneity.

4 Discussion

Coarse-resolution climate models have structural errors that arise due to their inability to resolve small-scale heterogeneity. The impacts of this missing sub-grid scale heterogeneity on the resolved state needs to be parameterized to reduce structural uncertainty and improve the fidelity of our future climate projections. Here we estimate the size and patterns of the air-sea turbulent heat flux that directly impacts the large-scale flow and is missing when small-scale heterogeneity is absent.

We find that this flux (Q^*) leads to a net cooling of the ocean, with the strongest cooling observed in the most dynamically active regions of the ocean, like the western boundary currents. Locally Q^* can be as large as O(100) W/m^2, while the long-term average cooling can be as large as 20-30 W/m^2 in some key regions. We also show that Q^* can be explained primarily as a sum of contributions from the oceanic (SST heterogeneity) and atmospheric (wind heterogeneity) small-scale heterogeneity. While this atmospheric contribution leads to cooling everywhere in the time average, the oceanic contribution is much more spatially variable and results in both cooling and warming. Some of these patterns of oceanic contribution seem to be correlated with known SST biases in current generation of climate models[39].

The novelty of our approach is that with the help of a high-resolution coupled simulation and the ability to compute air-sea fluxes offline, we were able to precisely isolate the impact of small-scale heterogeneity on air-sea heat flux. Past approaches, which compare model states across model resolutions or coupling resolutions, are unable to isolate the impact of individual processes; since changing resolution leads to changes in the strength and influence of many processes and also a change in the large-scale atmosphere and ocean state. However, this also highlights a few caveats of our study.

Firstly, our work relies on high-resolution coupled numerical models and the results are sensitive to the resolution of our model and scale of filtering. While we do not believe that the qualitative results of our study would change as these parameters are changed, we hope to build quantitative confidence by using higher-resolution coupled simulations and also address the scale-dependence of our estimated fluxes in future studies. In particular, it would be exciting to assess these processes in the new generation of ultra-high resolution global storm and eddy-resolving coupled simulations that are being developed as part of the second phase of DYAMOND[32]. Also, crucially, newly proposed satellite missions such as ODYSEA[35] and field campaigns conducting high-resolution surveys of the air-sea transition zone, which aim to measure both atmosphere and ocean states simultaneously, offer the opportunity to verify and quantify these impacts from observations.

Secondly, by design, we were able to study a single process in isolation, but more work needs to be done to understand how the missing flux that we have identified interacts with other processes and impacts the large-scale circulation and energetics. One direction in doing this would be to build a parameterization of the effect documented here, and to study the impact and connection of this parameterization with other model components. Conceptually the atmospheric contribution that we have estimated may be accounted for by gustiness parameterizations, but no equivalent parameterization exists to account for the impact of small-scale oceanic heterogeneity on air-sea fluxes. Also, while we have focussed on turbulent heat fluxes in this study, a natural next extension would be to study the effects on momentum or gas fluxes. We hope that these efforts could help reduce biases in future CMIP class simulations.

5 Methods

5.1 High-resolution simulation data

We use daily averaged output fields from the control runs of two global, high resolution, coupled, ocean-atmosphere climate model simulations. Both models are considered ocean eddy permitting with a nominal resolution of 0.1° in the ocean component. Since we find that our main conclusions are supported by both simulations (see Supplementary Material) we choose to present only results from the longer CM2.6 in the main text for simplicity.

CM2.6 The CM2.6 model configuration[13] is part of the suite of centennial-scale 1990 radiatively forced numerical climate simulations from three GFDL coupled models (CM2-O). The atmospheric resolution is nominally 0.5°. The output required for this study was availabe for the last 20 years of the 100 year simulation as daily averages.

CESM The Community Earth System Model version 1.1[27] (henceforth referred to simply as CESM) has a finer atmospheric resolution of 0.25°. We use daily average output from 2 years of a 100-year simulation, run under present-day (year 2000) conditions.

For this study we use Analysis-Ready Cloud Optimized (ARCO)[1] editions of these datasets in Zarr format ingested to cloud storage via Pangeo Forge[30].

5.2 Computing turbulent heat fluxes offline

Since we did our study using full resolution and filtered variables using archived climate model data, we had to recompute the turbulent air-sea heat fluxes offline (post simulation) using the same bulk-formulae that were used during simulation. These bulk-formulae algorithms for offline calculations have been made available as a Fortran package called Aerobulk (https://github.com/brodeau/aerobulk), by[5]. We created the aerobulk-python package[6], which provides python wrappers for the Fortran code.

The latent (Q_{lat}) and sensible (Q_{sen}) turbulent heat fluxes are computed using the bulk formulae ($A_{Bulk}(...)$) as follows:

$$Q_{lat}, Q_{sen} = A_{Bulk}(\theta_A, \theta_O, \mathbf{u}_A, \mathbf{u}_O, q_A, p_A), \tag{2}$$

where sub-script A and O correspond to atmospheric and oceanic variables near the air-sea interface, θ_f is the potential temperature in each fluid, $\mathbf{u}_f$ is the velocity in each fluid, q_A is the atmospheric relative humidity, and p_A is the atmospheric sea level pressure. The bulk formulae in fact only uses the relative wind ($\mathbf{u}_A - \mathbf{u}_O$) in all its internal calculations. The oceanic variables are passed as values in the top most ocean cell, and the atmospheric scalar variables (θ_A, q_A, p_A) are taken from fixed heights z_s and atmospheric velocity variables ($\mathbf{u}_A$) are taken from fixed height z_u. These heights are also passed as inputs to the bulk formulae. The bulk formulae are iterative solvers, and we used 6 iterations when doing the offline computations.

Interpolation The atmospheric and oceanic fields are not on the same grid, and need to be colocated before fluxes can be computed. Here, for the calculation of fluxes, we interpolate all atmospheric fields onto their corresponding ocean model grids using the xESMF-python package[16].

Given constraints on the available simulation output (archived data is daily averages, rather than snapshots) the heat fluxes calculated offline are sufficiently close to the fluxes computed during the simulation (see Supplementary Materials for details). Also, the results found in this study are qualitatively independent of the choice of algorithm (see Supplementary Material for a discussion of quantitative differences). We thus present results only for the `ecmwf` algorithm.

5.3 Computing impact of small scales on turbulent air-sea heat fluxes

In this study, we investigate whether the small-scale variability in the turbulent air-sea heat flux, generated due to the small-scale heterogeneity in the flow fields, results in a net flux at the large scales.

The latent (Q_{lat}) and sensible (Q_{sens}) turbulent heat fluxes defined in equation 5 are the fluxes composed of variability at all scales. The contributions of this full variability flux to the large-scale flux can be quantified by filtering (the details of the filter – $\overline{(.)}$ – are explained towards the end of this section), and this net flux is denoted as $\overline{Q_{lat}}$ and $\overline{Q_{sens}}$. A coarse-resolution model, which is unable to resolve the small-scale heterogeneity in the flow fields is only able to produce heat fluxes corresponding to low-resolution flow fields, which are computed as:

$$Q^c_{lat}, Q^c_{sens} = A_{Bulk}(\overline{\theta_A}, \overline{\theta_O}, \overline{\mathbf{u}_A}, \overline{\mathbf{u}_O}, \overline{q_A}, \overline{p_A}). \tag{3}$$

These are computed the same way as equation 5, but using filtered fields as input. If the bulk-formulae were linear functions, then $\overline{Q_{lat}}$, $\overline{Q_{sens}}$ would be the same as Q^c_{lat}, Q^c_{sens}. However, the non-linearities of bulk formulae imply that small-scale heterogeneity can interact and contribute to the net flux at the large-scales. We compute this contribution of small-scale heterogeneity to net large-scale flux as,

$$Q^*_{lat} = \overline{Q}_{lat} - \overline{Q^c}_{lat}, \tag{4}$$

$$Q^*_{sen} = \overline{Q}_{sen} - \overline{Q^c}_{sen}. \tag{5}$$

Note that here we have applied an additional spatial filter to the Q^c equations as well, because the non-linearities can produce variability at scales that should be smoothed out due to the filtered input variables to the bulk formulae. This way of defining the contribution of the small-scales follows from the large eddy simulation literature[38;22].

Filtering We filter high-resolution model fields to generate variables with reduced heterogeneity, such that they have similar smoothness to variables from a coarse-resolution model. Here we use spatial filtering to achieve this, with the help of a 2-dimensional Gaussian kernel filter implemented via the GCM-filters python package[14;19]. In this study we use a 2^o filter kernel, to generate filtered fields that roughly match what is produced by most current CMIP class models. As shown in the Supplementary Material, our main results are relatively independent of the filtering method, as long as roughly the same length scales are filtered.

5.4 Decomposing impact of small scales in to components from the Atmosphere and Ocean

The atmospheric and oceanic small-scales have very different spatio-temporal properties. Broadly speaking, the ocean small-scale correspond to slow time scales and small spatial scales, while the atmosphere small-scales are composed of faster time scales but relatively larger spatial scales. Thus, it is interesting to study the impacts of the small-scale heterogeneity in each fluid independently. Here we only show formulae for the latent heat fluxes, but same details would follow for sensible heat fluxes too.

To isolate the effects of small scales in the atmosphere, we first compute heat fluxes where only the atmospheric fields have been smoothed:

$$Q^{c,A}_{lat} = A_{Bulk}(\overline{\theta_A}, \theta_O, \overline{\mathbf{u}_A}, \mathbf{u}_O, \overline{q_A}, \overline{p}_A), \tag{6}$$

and the define the small-scale contribution as

$$Q^{*,A}_{lat} = \overline{Q}_{lat} - \overline{Q^{c,A}}_{lat} \tag{7}$$

Similarly the effects of the small-scales in the ocean are studied by first computing fluxes with only coarsening the oceanic fields:

$$Q^{c,O}_{lat} = A_{Bulk}(\theta_A, \overline{\theta_O}, \mathbf{u}_A, \overline{\mathbf{u}_O}, q_A, p_A), \tag{8}$$

and then defining the small scale contribution as

$$Q^{*,O}_{lat} = \overline{Q}_{lat} - \overline{Q^{c,O}}_{lat}. \tag{9}$$

Note that the impact of the coupled small-scale features is defined as the residual

$$Q^{*,O-A}_{lat} = Q^*_{lat} - Q^{*,O}_{lat} - Q^{*,A}_{lat}. \tag{10}$$

It should be noted that some degree of small-scale heterogeneity in the atmosphere or the ocean flow fields may be generated by coupling between the two fluids, while a large part of it is created by the intrinsic variability of the two fluids. $Q_{lat}^{*,O-A}$ is not a measure of the flux resulting from the heterogeneity generated by coupling, as the impact of this small-scale heterogeneity (even though generated in response to coupling), has been accounted for in either $Q_{lat}^{*,O}$ or $Q_{lat}^{*,A}$. Rather, $Q_{lat}^{*,O-A}$ accounts only for the flux impact that results due to the small-scale correlation and its projection onto the flux between the two fluids.

5.5 Data Availability

The code to reproduce our resutls can be found on github https://github.com/ocean-transport/scale-aware-air-sea and will additionally be archived on zenodo before publication. The raw data used in this study is available in cloud storage (urls can be found in the above code).

Acknowledgments

JB, PM, TN, RA were supported by the Gordon and Betty Moore Foundation (Award 8434). CS was supported by the National Science Foundation Grant No. 2026932. We acknowledge the computing and storage resources provided by the 'NSF Science and Technology Center (STC) Learning the Earth with Artificial intelligence and Physics (LEAP)' (Award No. 2019625). JB, DB and RA received support through Schmidt Sciences.

Author Contributions

JB conducted the analysis, generated the figures, interpreted the results and wrote the manscript. DB helped with the analysis, interpreting the results, and writing the manuscript. PM helped with the analysis, interpreting the results, and writing the manuscript. TN helped in development of the computational pipelines for offline computation of fluxes. ZJ helped in developing robust approaches for flux decomposition. CS helped with making the essential data available on the cloud. RA concieved the idea for the project, helped to interpret results, and contributed to manuscript writing.

References

[1] Ryan P Abernathey, Tom Augspurger, Anderson Banihirwe, Charles C Blackmon-Luca, Timothy J Crone, Chelle L Gentemann, Joseph J Hamman, Naomi Henderson, Chiara Lepore, Theo A McCaie, et al. Cloud-native repositories for big scientific data. *Computing in Science & Engineering*, 23(2):26–35, 2021.

[2] Julie Bessac, Hannah M Christensen, Kota Endo, Adam H Monahan, and Nils Weitzel. Scale-aware space-time stochastic parameterization of subgrid-scale velocity enhancement of sea surface fluxes. *Journal of Advances in Modeling Earth Systems*, 13(4):e2020MS002367, 2021.

[3] Stuart P Bishop, R Justin Small, and Frank O Bryan. The global sink of available potential energy by mesoscale air-sea interaction. *Journal of Advances in Modeling Earth Systems*, 12(10): e2020MS002118, 2020.

[4] Sébastien Blein, Romain Roehrig, Aurore Voldoire, and Ghislain Faure. Meso-scale contribution to air–sea turbulent fluxes at gcm scale. *Quarterly Journal of the Royal Meteorological Society*, 146(730):2466–2495, 2020.

[5] Laurent Brodeau, Bernard Barnier, Sergey K Gulev, and Cian Woods. Climatologically significant effects of some approximations in the bulk parameterizations of turbulent air–sea fluxes. *Journal of Physical Oceanography*, 47(1):5–28, 2017.

[6] Julius J. M. Busecke, Paige E. Martin, and Ryan P. Abernathey. aerobulk-python, May 2024. URL https://doi.org/10.5281/zenodo.11205116.

[7] Hannah Christensen and Laure Zanna. Parametrization in weather and climate models. 2022.

[8] Carol Anne Clayson, Charlotte Demott, S De Szoeke, Ping Chang, Gregory R Foltz, Raghavendra Krishnamurthy, Tong Lee, Andrea M Molod, David Ortiz-Suslow, Julie Pullen, et al. A new paradigm for observing and modeling of air-sea interactions to advance earth system prediction. Technical report, Pacific Northwest National Laboratory (PNNL), Richland, WA (United States), 2023.

[9] Meghan F Cronin, Chelle L Gentemann, James Edson, Iwao Ueki, Mark Bourassa, Shannon Brown, Carol Anne Clayson, Chris W Fairall, J Thomas Farrar, Sarah T Gille, et al. Air-sea fluxes with a focus on heat and momentum. *Frontiers in Marine Science*, 6:430, 2019.

[10] V. Eyring, S. Bony, G. A. Meehl, C. A. Senior, B. Stevens, R. J. Stouffer, and K. E. Taylor. Overview of the coupled model intercomparison project phase 6 (cmip6) experimental design and organization. *Geoscientific Model Development*, 9(5):1937–1958, 2016. doi: 10.5194/gmd-9-1937-2016. URL https://gmd.copernicus.org/articles/9/1937/2016/.

[11] Kirsten L Findell, Zun Yin, Eunkyo Seo, Paul A Dirmeyer, Nathan P Arnold, Nathaniel Chaney, Megan D Fowler, Meng Huang, David M Lawrence, Po-Lun Ma, et al. Accurate assessment of land–atmosphere coupling in climate models requires high-frequency data output. *Geoscientific Model Development*, 17(4):1869–1883, 2024.

[12] JS Godfrey and ACM Beljaars. On the turbulent fluxes of buoyancy, heat and moisture at the air-sea interface at low wind speeds. *Journal of Geophysical Research: Oceans*, 96(C12):22043–22048, 1991.

[13] Stephen M. Griffies, Michael Winton, Whit G. Anderson, Rusty Benson, Thomas L. Delworth, Carolina O. Dufour, John P. Dunne, Paul Goddard, Adele K. Morrison, Anthony Rosati, Andrew T. Wittenberg, Jianjun Yin, and Rong Zhang. Impacts on ocean heat from transient mesoscale eddies in a hierarchy of climate models. *Journal of Climate*, 28(3):952–977, February 2015. ISSN 1520-0442. doi: 10.1175/jcli-d-14-00353.1. URL http://dx.doi.org/10.1175/JCLI-D-14-00353.1.

[14] Ian Grooms, Nora Loose, Ryan Abernathey, JM Steinberg, Scott Daniel Bachman, Gustavo Marques, Arthur Paul Guillaumin, and Elizabeth Yankovsky. Diffusion-based smoothers for spatial filtering of gridded geophysical data. *Journal of Advances in Modeling Earth Systems*, 13(9): e2021MS002552, 2021.

[15] Helene Hewitt, Baylor Fox-Kemper, Brodie Pearson, Malcolm Roberts, and Daniel Klocke. The small scales of the ocean may hold the key to surprises. *Nature Climate Change*, 12(6):496–499, June 2022. ISSN 1758-6798. doi: 10.1038/s41558-022-01386-6. URL http://dx.doi.org/10.1038/s41558-022-01386-6.

[16] Jiawei Zhuang, Raphael Dussin, David Huard, Pascal Bourgault, Anderson Banihirwe, Stephane Raynaud, Brewster Malevich, Martin Schupfner, , Filipe, Sam Levang, Charles Gauthier, André Jüling, Mattia Almansi, RichardScottOZ, RondeauG, Stephan Rasp, Trevor James Smith, Jemma Stachelek, Matthew Plough, , Pierre, Ray Bell, Romain Caneill, and Xianxiang Li. pangeo-data/xesmf: v0.8.2, 2023. URL https://zenodo.org/record/4294774.

[17] Gregory C. Johnson, Rick Lumpkin, Tim Boyer, Francis Bringas, Ivona Cetinić, Don P. Chambers, Lijing Cheng, Shenfu Dong, Richard A. Feely, Baylor Fox-Kemper, Eleanor Frajka-Williams, Bryan A. Franz, Yao Fu, Meng Gao, Jay Garg, John Gilson, Gustavo Goni, Benjamin D. Hamlington, Helene T. Hewitt, William R. Hobbs, Zeng-Zhen Hu, Boyin Huang, Svetlana Jevrejeva, William E. Johns, Sato Katsunari, John J. Kennedy, Marion Kersalé, Rachel E. Killick, Eric Leuliette, Ricardo Locarnini, M. Susan Lozier, John M. Lyman, Mark A. Merrifield, Alexey Mishonov, Gary T. Mitchum, Ben I. Moat, R. Steven Nerem, Dirk Notz, Renellys C. Perez, Sarah G. Purkey, Darren Rayner, James Reagan, Claudia Schmid, David A. Siegel, David A. Smeed, Paul W. Stackhouse, William Sweet, Philip R. Thompson, Denis L. Volkov, Rik Wanninkhof, Robert A. Weller, Caihong Wen, Toby K. Westberry, Matthew J. Widlansky, Josh K. Willis, Lisan Yu, and Huai-Min Zhang. Global oceans. *Bulletin of the American Meteorological Society*, 103(8):S143–S192, August 2022. ISSN 1520-0477. doi: 10.1175/bams-d-22-0072.1. URL http://dx.doi.org/10.1175/BAMS-D-22-0072.1.

[18] Norman G Loeb, Gregory C Johnson, Tyler J Thorsen, John M Lyman, Fred G Rose, and Seiji Kato. Satellite and ocean data reveal marked increase in earth's heating rate. *Geophysical Research Letters*, 48(13):e2021GL093047, 2021.

[19] Nora Loose, Ryan Abernathey, Ian Grooms, Julius Busecke, Arthur Guillaumin, Elizabeth Yankovsky, Gustavo Marques, Jacob Steinberg, Andrew Slavin Ross, Hemant Khatri, et al. Gcm-filters: A python package for diffusion-based spatial filtering of gridded data. *Journal of Open Source Software*, 7(70):3947, 2022.

[20] Thomas Rackow and Stephan Juricke. Flow-dependent stochastic coupling for climate models with high ocean-to-atmosphere resolution ratio. *Quarterly Journal of the Royal Meteorological Society*, 146(726):284–300, November 2019. ISSN 1477-870X. doi: 10.1002/qj.3674. URL http://dx.doi.org/10.1002/qj.3674.

[21] Shikhar Rai, Matthew Hecht, Matthew Maltrud, and Hussein Aluie. Scale of oceanic eddy killing by wind from global satellite observations. *Science Advances*, 7(28):eabf4920, 2021.

[22] Pierre Sagaut. *Large eddy simulation for incompressible flows: an introduction*. Springer Science & Business Media, 2005.

[23] Lauren Schmeisser, Nicholas A. Bond, Samantha A. Siedlecki, and Thomas P. Ackerman. The role of clouds and surface heat fluxes in the maintenance of the 2013–2016 northeast pacific marine heatwave. *Journal of Geophysical Research: Atmospheres*, 124(20):10772–10783, October 2019. ISSN 2169-8996. doi: 10.1029/2019jd030780. URL http://dx.doi.org/10.1029/2019JD030780.

[24] Tapio Schneider, Shiwei Lan, Andrew Stuart, and João Teixeira. Earth system modeling 2.0: A blueprint for models that learn from observations and targeted high-resolution simulations. *Geophysical Research Letters*, 44(24), December 2017. ISSN 1944-8007. doi: 10.1002/2017gl076101. URL http://dx.doi.org/10.1002/2017GL076101.

[25] Richard Seager, Mark Cane, Naomi Henderson, Dong-Eun Lee, Ryan Abernathey, and Honghai Zhang. Strengthening tropical pacific zonal sea surface temperature gradient consistent with rising greenhouse gases. *Nature Climate Change*, 9(7):517–522, 2019.

[26] Hyodae Seo, Larry W O'Neill, Mark A Bourassa, Arnaud Czaja, Kyla Drushka, James B Edson, Baylor Fox-Kemper, Ivy Frenger, Sarah T Gille, Benjamin P Kirtman, et al. Ocean mesoscale and frontal-scale ocean–atmosphere interactions and influence on large-scale climate: A review. *Journal of climate*, 36(7):1981–2013, 2023.

[27] R. Justin Small, Julio Bacmeister, David Bailey, Allison Baker, Stuart Bishop, Frank Bryan, Julie Caron, John Dennis, Peter Gent, Hsiao-ming Hsu, Markus Jochum, David Lawrence, Ernesto Muñoz, Pedro diNezio, Tim Scheitlin, Robert Tomas, Joseph Tribbia, Yu-heng Tseng, and Mariana Vertenstein. A new synoptic scale resolving global climate simulation using the community earth system model. *Journal of Advances in Modeling Earth Systems*, 6(4):1065–1094, 2014. doi: https://doi.org/10.1002/2014MS000363.

[28] R. Justin Small, Frank O. Bryan, Stuart P. Bishop, Sarah Larson, and Robert A. Tomas. What drives upper-ocean temperature variability in coupled climate models and observations? *Journal of Climate*, 33(2):577–596, January 2020. ISSN 1520-0442. doi: 10.1175/jcli-d-19-0295.1. URL http://dx.doi.org/10.1175/JCLI-D-19-0295.1.

[29] RJ d Small, Simon P deSzoeke, SP Xie, L O'neill, H Seo, Q Song, P Cornillon, M Spall, and S Minobe. Air–sea interaction over ocean fronts and eddies. *Dynamics of Atmospheres and Oceans*, 45(3-4):274–319, 2008.

[30] Charles Stern, Ryan Abernathey, Joseph Hamman, Rachel Wegener, Chiara Lepore, Sean Harkins, and Alexander Merose. Pangeo forge: Crowdsourcing analysis-ready, cloud optimized data production. *Frontiers in Climate*, 3, 2022. ISSN 2624-9553. doi: 10.3389/fclim.2021.782909. URL https://www.frontiersin.org/articles/10.3389/fclim.2021.782909.

[31] Bjorn Stevens and Sandrine Bony. What are climate models missing? *Science*, 340(6136): 1053–1054, May 2013. ISSN 1095-9203. doi: 10.1126/science.1237554. URL http://dx.doi.org/10.1126/science.1237554.

[32] Bjorn Stevens, Masaki Satoh, Ludovic Auger, Joachim Biercamp, Christopher S Bretherton, Xi Chen, Peter Düben, Falko Judt, Marat Khairoutdinov, Daniel Klocke, et al. Dyamond: the dynamics of the atmospheric general circulation modeled on non-hydrostatic domains. *Progress in Earth and Planetary Science*, 6(1):1–17, 2019.

[33] Ehud Strobach, Patrice Klein, Andrea Molod, Abdullah A. Fahad, Atanas Trayanov, Dimitris Menemenlis, and Hector Torres. Local air-sea interactions at ocean mesoscale and submesoscale in a western boundary current. *Geophysical Research Letters*, 49(7), March 2022. ISSN 1944-8007. doi: 10.1029/2021gl097003. URL http://dx.doi.org/10.1029/2021GL097003.

[34] Rui Sun, Aneesh C Subramanian, Bruce D Cornuelle, Matthew R Mazloff, Arthur J Miller, F Martin Ralph, Hyodae Seo, and Ibrahim Hoteit. The role of air–sea interactions in atmospheric rivers: Case studies using the SKRIPS regional coupled model. *J. Geophys. Res.*, 126(6), March 2021.

[35] Hector Torres, Alexander Wineteer, Patrice Klein, Tong Lee, Jinbo Wang, Ernesto Rodriguez, Dimitris Menemenlis, and Hong Zhang. Anticipated capabilities of the odysea wind and current mission concept to estimate wind work at the air–sea interface. *Remote Sensing*, 15(13), 2023. ISSN 2072-4292. doi: 10.3390/rs15133337. URL https://www.mdpi.com/2072-4292/15/13/3337.

[36] Igor Uchoa, Jacob O Wenegrat, and Lionel Renault. Sink of eddy energy by submesoscale sea surface temperature variability in a coupled regional model. 2024.

[37] Paul D. Williams. Climatic impacts of stochastic fluctuations in air–sea fluxes. *Geophysical Research Letters*, 39(10), May 2012. ISSN 1944-8007. doi: 10.1029/2012gl051813. URL http://dx.doi.org/10.1029/2012GL051813.

[38] GS Winckelmans, TS Lund, Daniele Carati, and AA Wray. A priori testing of subgrid-scale models for the velocity-pressure and vorticity-velocity formulations. *Studying Turbulence Using Numerical Simulation Databases*, 1996.

[39] Qibei Zhang, Bo Liu, Shuanglin Li, and Tianjun Zhou. Understanding models' global sea surface temperature bias in mean state: From cmip5 to cmip6. *Geophysical Research Letters*, 50(4), February 2023. ISSN 1944-8007. doi: 10.1029/2022gl100888. URL http://dx.doi.org/10.1029/2022GL100888.

Supplementary Material for: The Overlooked Sub-Grid Air-Sea Flux in Climate Models

Julius J.M. Busecke[†*1], Dhruv Balwada[†1], Paige E. Martin[1], Thomas E.G. Nicholas[1], Zoe C.P. Johnson[2], Charles I. Stern[1], and Ryan P. Abernathey[1]

[1]Lamont Doherty Earth Observatory, Columbia University, Palisades, NY, USA
[3]Barnard College of Columbia University, New York, NY, USA

1 Temporal averaging and areas covered in sea ice

The bulk algorithms as implemented in this study do not support calculating fluxes in the presence of sea ice, and thus we need to mask input data values that might be affected by sea-ice. Neither of the simulations provides sea ice concentrations as output, and we approximate a mask by eliminating grid cells that have a sea surface temperature below 0°C. All values identified by that mask are removed.

This means that long term means in the area of seasonal sea ice occurence represent less data points than on the open ocean. It also means that the order of time averaging and spatial filtering of turbulent heatfluxes does not commute at the sea-ice edge, since it is a non-stationary boundary.

We compute all time averaged ($\overline{(.)}^T$) results shown in the main manuscript as the sum of the time averaged components.

$$\overline{Q^*}^T = \overline{Q^*_{lat}}^T + \overline{Q^*_{sen}}^T \tag{1}$$

For each component (only shown for sensible heatflux) we compute the time average as

$$\overline{Q^*_{sen}}^T = \overline{\overline{Q_{sen}}^T} - \overline{\overline{Q^c}_{sen}^T}, \tag{2}$$

rather than

$$\overline{Q^*_{sen}}^T = \overline{\overline{Q_{sen}}}^T - \overline{\overline{Q^c}_{sen}}^T, \tag{3}$$

since this saves many computationally expensive filtering steps.

Figure 1 demonstrates on a 1 year dataset, that in the open ocean these two ways methods are indeed equivalent for $\overline{Q^*}^T$, and differences are contained to the area covered by the moving ice edge and are small compared to the results presented in the main manuscript, especially when averaged globally.

To indicate areas that might be influenced by the presence of sea ice we indicate the maximum extent of the sea ice edge with an orange contour in each map plot. Additionally we compute global averages in those plots for all values and only for values that are never covered by sea-ice (values in parentheses on the upper left edge of each map).

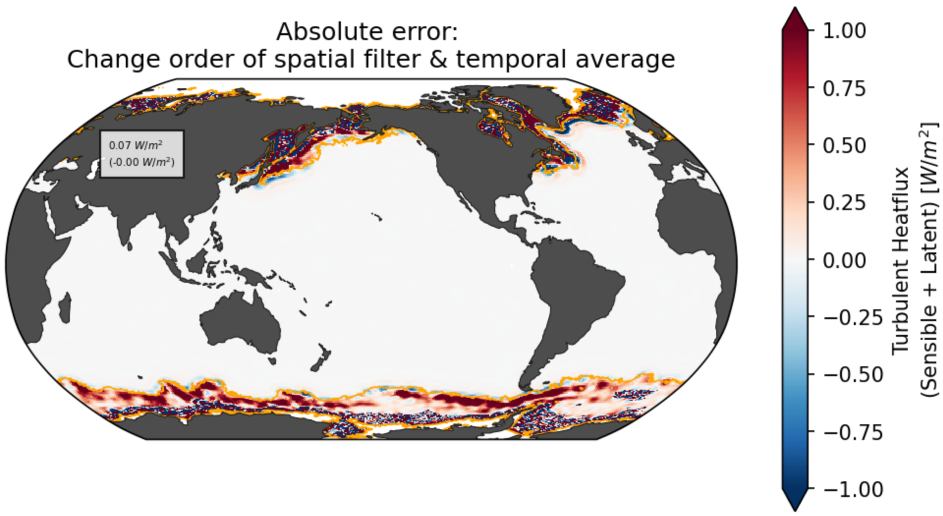

Figure 1: Absolute difference between Q^* when changing the order of temporal averaging and spatial filtering (see Equation 2 and 3). The averaging is done over the first year of the CM2.6 simulation. Orange lines indicate the maximum extent of sea ice. Numbers shown in the top left of map panels indicate global averaged values for all available values and only ice free locations in parentheses. For details on treamtment of sea ice and temporal averaging see Temporal averaging and areas covered in sea ice.

We find that none of our conclusions are changed by excluding areas that are partially covered by sea ice and in the text we exclusively refer to the values including all available data points.

2 Daily examples of Q^*

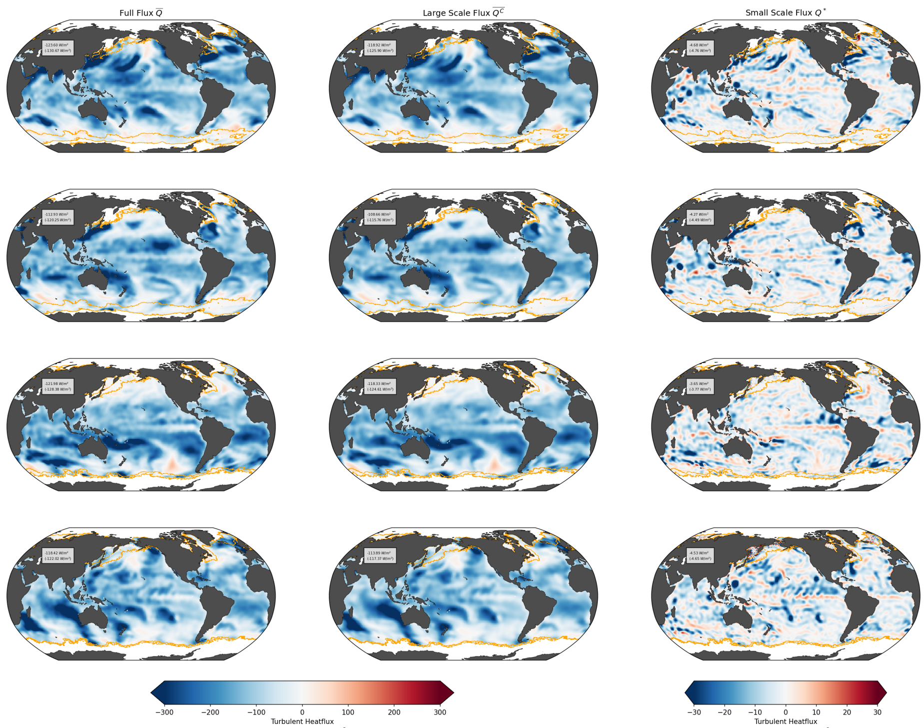

Figure 2: Daily flux maps for CM2.6. The columns indicate the different terms used in the study (see methods for details). **Left**: The smoothed full resolution flux $\overline{Q}$.; **Center**: The large scale flux ($\overline{Q^C}$) (Q_L_bar); **Right**:The small scale flux (Q^*). Each row shows the same daily timestep within the first year of the CM2.6 simulation. Orange lines indicate the maximum extent of sea ice. Numbers shown in the top left of map panels indicate global averaged values for all available values and only ice free locations in parentheses. For details on treamtment of sea ice and temporal averaging see Temporal averaging and areas covered in sea ice.

†These authors contributed equally to this work.
*Corresponding author: julius@ldeo.columbia.edu

Figure 2 shows several examples of $\overline{Q}$, $\overline{Q^C}$, and Q^* based on daily averages (the finest time frequency available for both simulations). These high time resolution fields show a large degree of variability particularly in Q^*, but also illustrate that many Q^* anomalies are associated with anomalies of the same sign in the $\overline{Q^C}*$ terms, and thus act to enhance the background variability.

3 Comparing offline and online fluxes

Our offline flux calculations are close to the values produced within the simulation itself. Figure 3 shows a close match of regional patterns for each simulation.

For CM2.6 our offline estimates however underestimate the global heatflux as a result of an underestimation of the latent heatflux and a lesser overestimation of the sensible heatflux (Figure 4). We note however that the mismatch between the offline and online latent heatfluxes for CM2.6 is about the same order of magnitude (10 W/m$\hat{2}$) as the difference between the online fluxes computed by the two simulations.

Possible issues leading to the mismatch could be:

- Nonlinear effects throughout the daily cycle, which we cannot capture due to the output frequency (daily average) of both simulations used here
- Corrections for skin temperature which were not implemented as part of this study.

For CESM (Figure 4, bottom row) the online flux is well captured by the range of offline fluxes, and due to the fact that all of our main results presented in the main manuscript are qualitatively the same for both simulations, we believe that the mismatch observed is of minor importance for the results presented in the manuscript.

4 Dependence on the choice of algorithm and smoothing method

Within the main manuscript we only present a single estimate of the small scale flux for brevity. To evaluate the sensitivity of our results to the choice of bulk algorithm and the two different smoothing methods, spatial filtering and coarse-graining, we repeated the analsyis for a shorter 1 year time window with all options. Due to the lack of strong interannual variability we believe these results to be representative of the full results. Figure 5 shows that the choice of algorithm changes results within a range of about $1W/m^2$, and the algorithm presented in the main manuscript (`ecmwf`) can be considered one of the more conservative estimates. We find that all conclusions of the main manuscript are very consistent across different algorithms, and thus are convinced that our results capture an actual physical mechanism, and that the choice of algorithm plays a secondary role for these findings. These conclusions also hold for the smoothing method, but coarsening generally leads to a larger small scale flux. This is likely due to the fact that coarsening removes more small scale variance compared to a Gaussian filter with the same window length.We chose the spatial filtering, since it enables the selective filtering of a subset of inputs, and thus decompose results into oceanic and atmospheric contributions, which is not possible with coarse graining.

4.1 Decomposition ocean/atmos vs tracer/vel

We extend the approach in Atmosphere and Ocean decomposition to decompose the small scale flux into contributions from tracers and velocity components. To isolate the effects of small scales in the

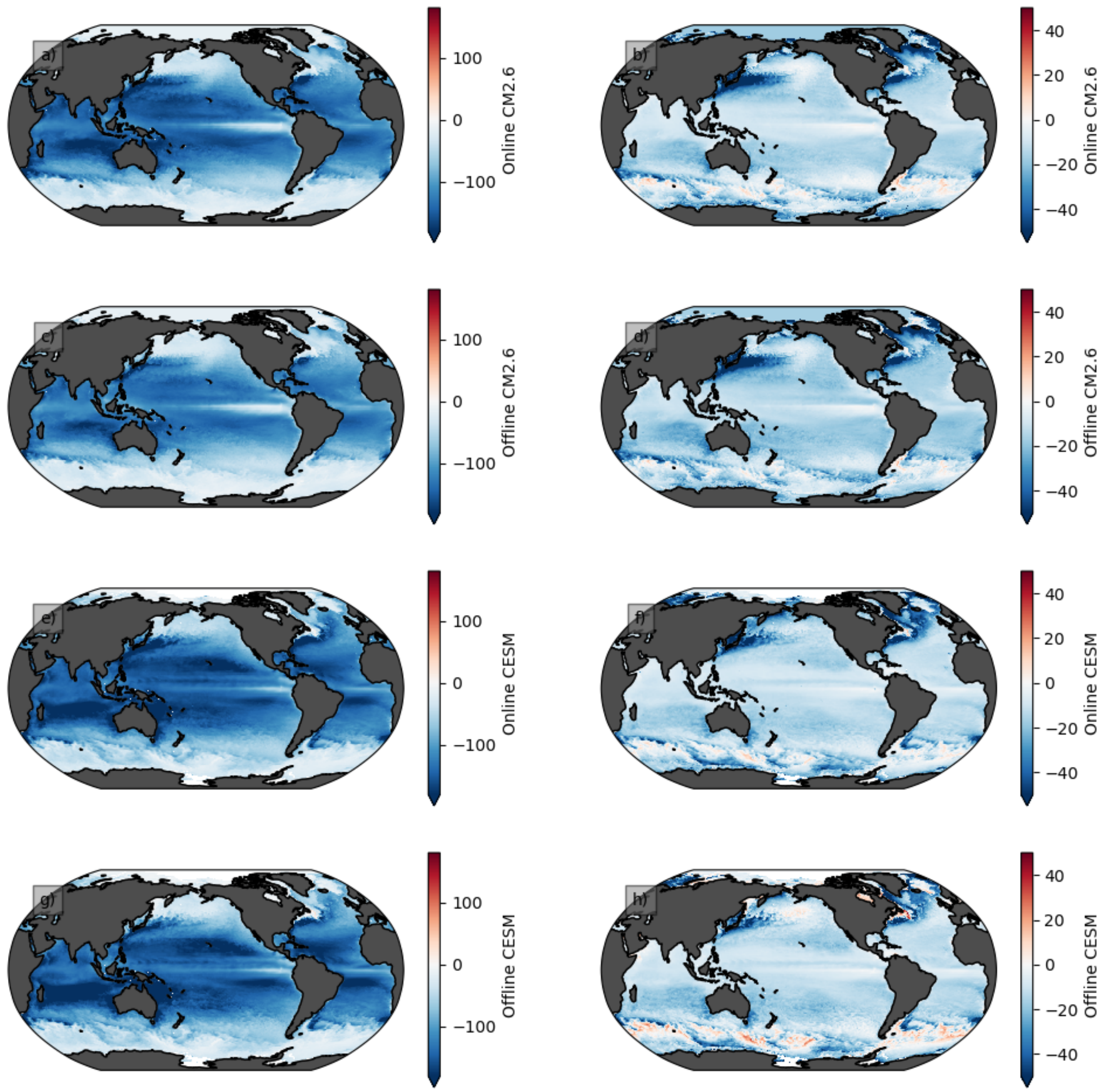

Figure 3: One year averaged heat fluxes (unsmoothed) for CM2.6 (a-d) and CESM (e-h). The **left column** shows the latent heatflux, and the **right column** shows the sensible heatflux.
a-d Show results for CM2.6. Panels a/b show the online fluxes (provided as part of the simulation output) and panels c/d show the offline fluxes (calculated via aerobulk-python). **e-h** Show results for CESM. Panels e/f show the online fluxes (provided as part of the simulation output) and panels g/h show the offline fluxes (calculated via aerobulk-python).

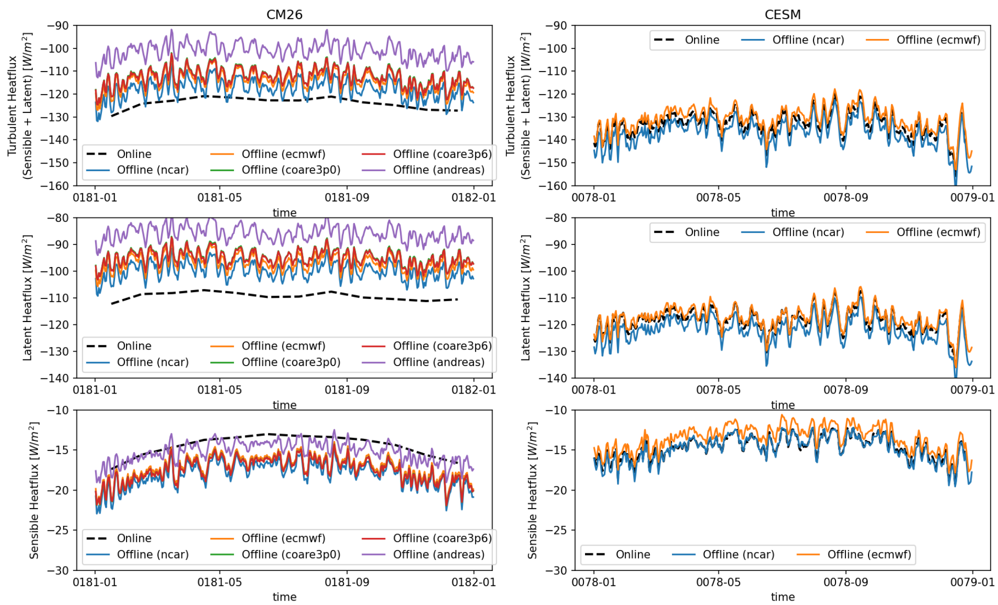

Figure 4: Timeseries of globally averaged full heat fluxes for CM2.6 (left column) and CESM (right column). The **upper row** shows latent heat flux, the **center row** shows sensible heatflux, and the **bottom row** shows the combined turbulent heatflux. The colored lines represent different algorithms used to calculate offline fluxes, and the black dashed line shows the flux output from the coupled simulation.

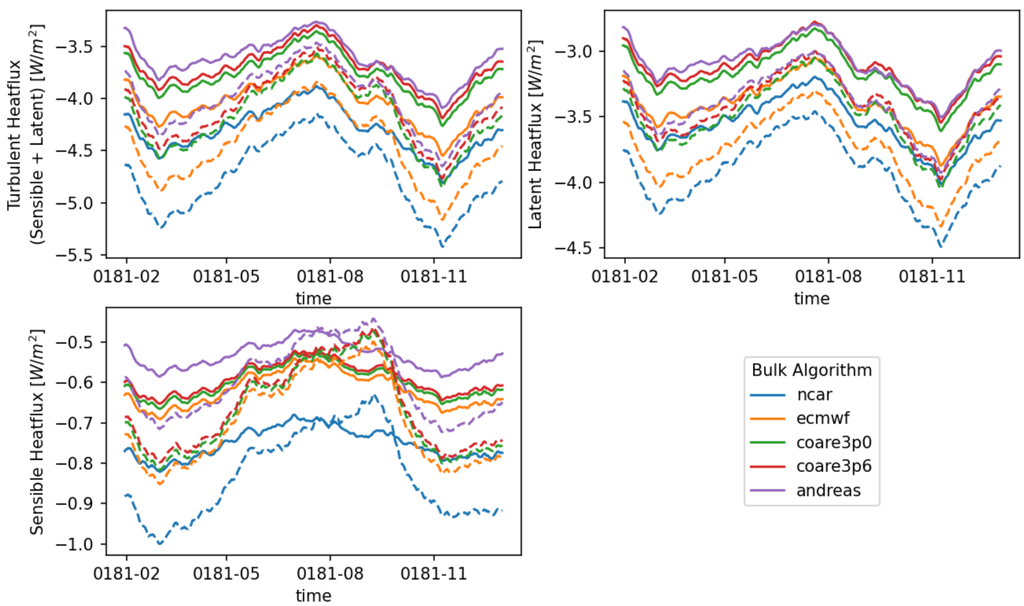

Figure 5: Global averaged small scale flux using different bulk algorithms and smoothing methods for the first year of the CM2.6 simulation. **Upper left**: Combined turbulent small scale flux Q^*. **Upper right**: Latent component of the small scale flux Q^*_{lat}. **Lower left**: Sensible component of the small scale flux Q^*_{sen}. (For definitions see the Methods section). Colors indicate the bulk algorithms used. The linestye indicates the smoothing method, solid lines for filtering (used in the manuscript) and dashed lines for coarsening.

velocity fields of both ocean and atmosphere compared to the effects of small scales in the tracer fields, we follow the same pattern in Eq 6-10 in the main manuscript.

To isolate the effects of small scales in the velocity, we first compute heat fluxes where only the velocity fields have been smoothed:

$$Q^{c,V}_{lat} = A_{Bulk}(\theta, \theta_O, \overline{\mathbf{u}_A}, \overline{\mathbf{u}_O}, q_A, p_A), \tag{4}$$

and the define the small-scale contribution as

$$Q^{*,V}_{lat} = \overline{Q}_{lat} - \overline{Q^{c,V}}_{lat} \tag{5}$$

Similarly the effects of the small-scales in the tracers of both ocean and atmosphere are quantified by first computing fluxes with only coarsening the tracer fields:

$$Q^{c,T}_{lat} = A_{Bulk}(\overline{\theta_A}, \overline{\theta_O}, \mathbf{u}_A, \mathbf{u}_O, \overline{q_A}, \overline{p_A}), \tag{6}$$

and then defining the small scale contribution as

$$Q^{*,T}_{lat} = \overline{Q}_{lat} - \overline{Q^{c,T}}_{lat}. \tag{7}$$

Figure 6 compares the decomposition into atmosphere and ocean contribution to the decomposition into velocity and tracer contributions. The pattern and global average values of the atmosphere and velocity contribution, and the ocean and tracer contribution are very similar. These results suggest the atmospheric contribution to be largely driven by the velocity contribution, whereas the oceanic contribution is largely driven by small scale tracer structures. This seems overall plausible. The atmospheric flow is generally much faster and shows high variability in velocities, but tracers like temperature tend to have larger scales than e.g. the SST in the ocean.

All of the above findings are qualitatevly consistent between the two simulations (results for CESM not shown).

4.2 Main conclusions from the paper for CESM

All conclusions drawn from the CM2.6 simulation are qualitatively supported by the CESM simulation. In fact, the values from CESM generally show a higher small scale flux contribution both locally and for the global mean. Figure 7 shows similar patterns for the small scale heatflux with strong enhancement in the western boundary currents, near the Equator and around the subpolar front. CESM also shows the dampening of air-sea fluxes near the equator. Overall the pattern seems noisier, particularly in the Southern Ocean, likely a consequence of the shorter simulation duration, where transient features might average out over time.

Just like the results presented in the main manuscript, the small scale flux does mostly reinforce the large scale heat flux, and a substantial amount (20+%) of local values enhance the large scale flux by more than 10% (Figure 8). We also see that within the Western Boundary current regions, the enhancement is even more pronounced, just like for CM2.6.

4.3 Interannual variability

We find that interannual variability in the globally averaged results is very small, making our choice of a single year to demonstrate the characteristics of daily results, as well as various analyses within this Supplementary Material, representative of the longer 20 year simulation.

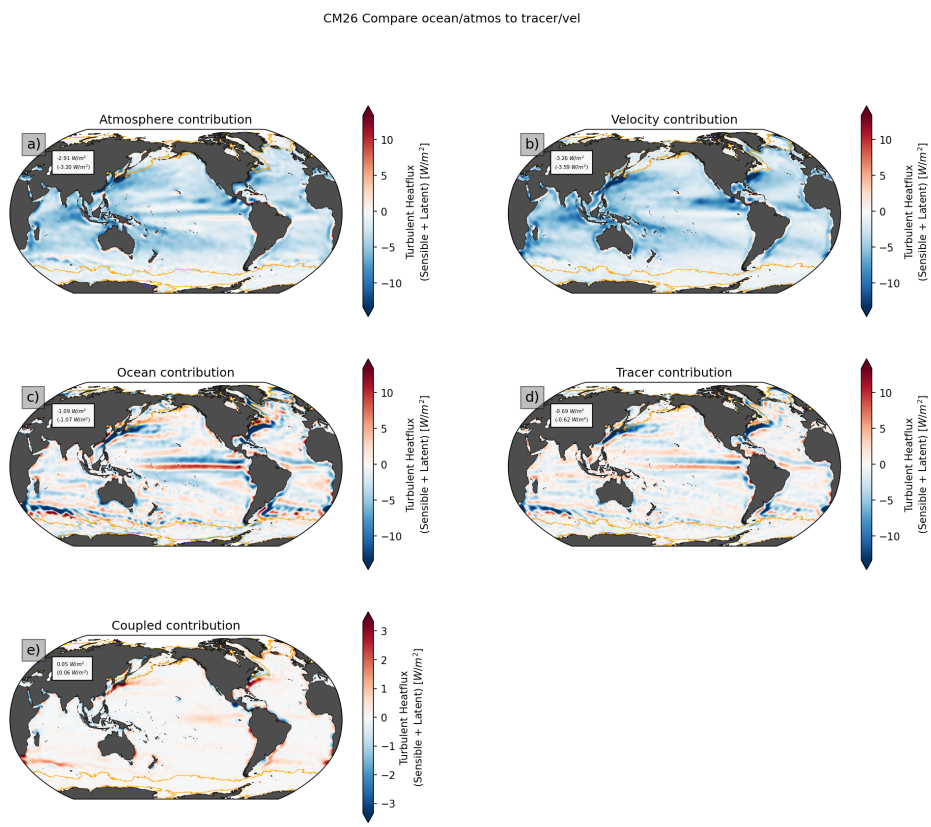

Figure 6: Comparison of the small scale ocean/atmosphere decomposition (left; similar as shown in Figure 4 of the main text) and tracer/velocity decomposition (right) for CM2.6. All terms are averaged over the first year of the simulation using the ecmwf algorithm. Orange lines indicate the maximum extent of sea ice. Numbers shown in the top left of map panels indicate global averaged values for all available values and only ice free locations in parentheses. For details on treamtment of sea ice and temporal averaging see Temporal averaging and areas covered in sea ice.

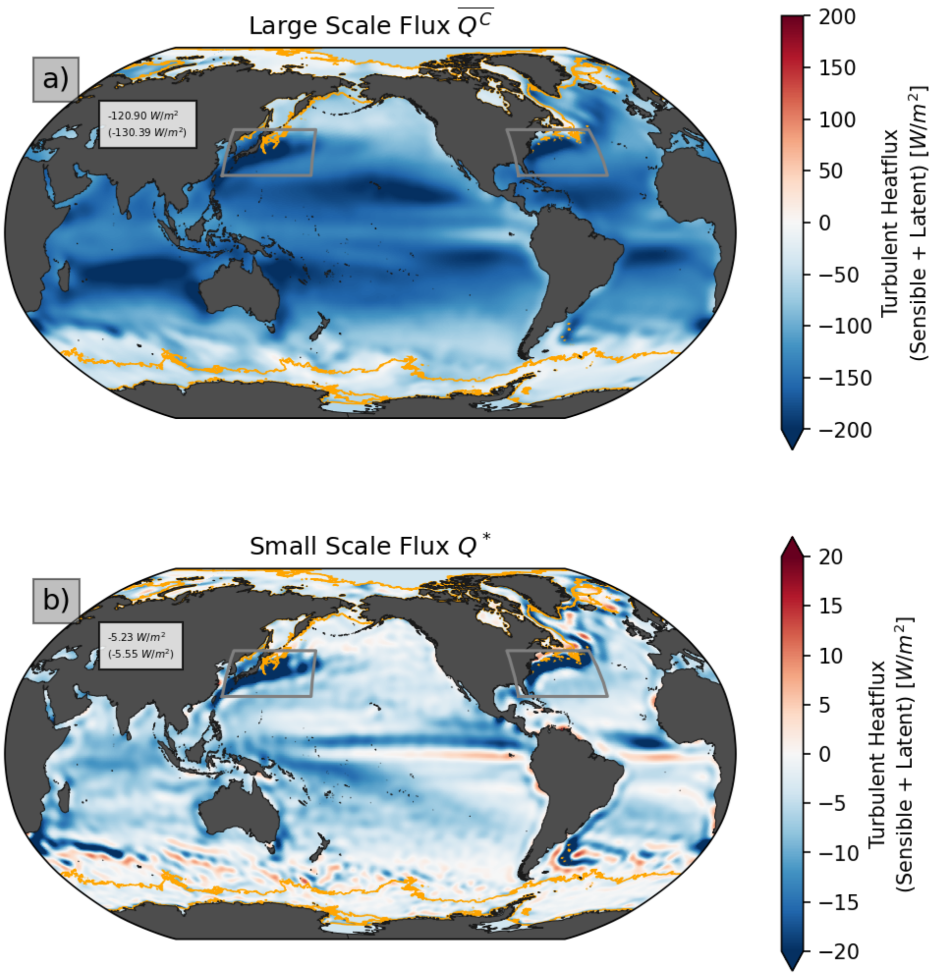

Figure 7: As Figure 2 in main manuscript but shows 20 year averaged results for CESM simulation. **a)** shows the large scale flux $\overline{Q^C}$ and **b)** shows the small scale flux Q^* (for details see Equation 1 in main manuscript). Negative values indicate ocean heat loss. Grey boxes indicate the Western Boundary Current regions used in Figure 8. Orange lines indicate the maximum extent of sea ice. Numbers shown in the top left of map panels indicate global averaged values for all available values and only ice free locations in parentheses. For details on treamtment of sea ice and temporal averaging see Temporal averaging and areas covered in sea ice.

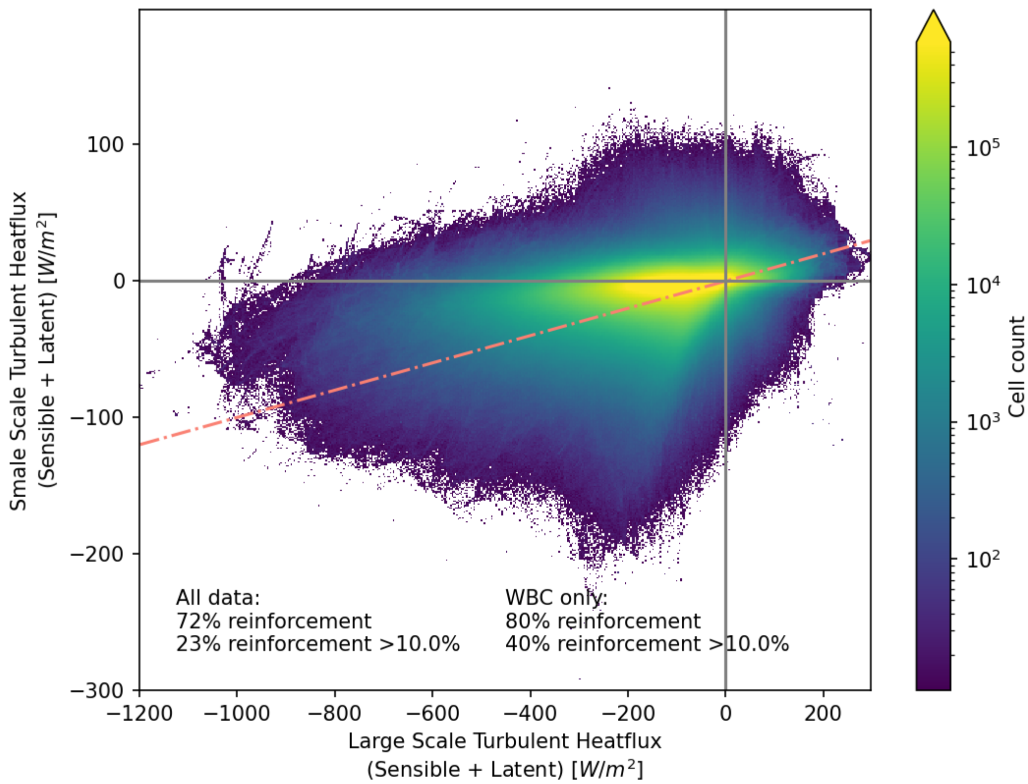

Figure 8: As Figure 3 in main manuscript but for CESM simulation. Bivariate histogram showing the relationship between the large-scale flux ($\overline{Q^C}$ on the x axis and the small scale flux Q^* on the y axis. Points falling in the upper-right and lower-left quadrant (same sign) indicate that the small scale flux is enhancing the large scale flux. Points falling below (above) the red dashed line in the lower-left (upper-right) quadrant are enhancing the large-scale flux by more than 10%. The percentages of total datapoints categorized as enhancing (enhancing more than 10%) are shown in the lower left of each panel. Text insets indicate the percentage of data points falling into these two categories for all data and only the northern Western Boundary current regions indicated in Figure 7. Note that the year to year variability is small (see Supplementary Material) and thus this relationship is representative of the full time frame.

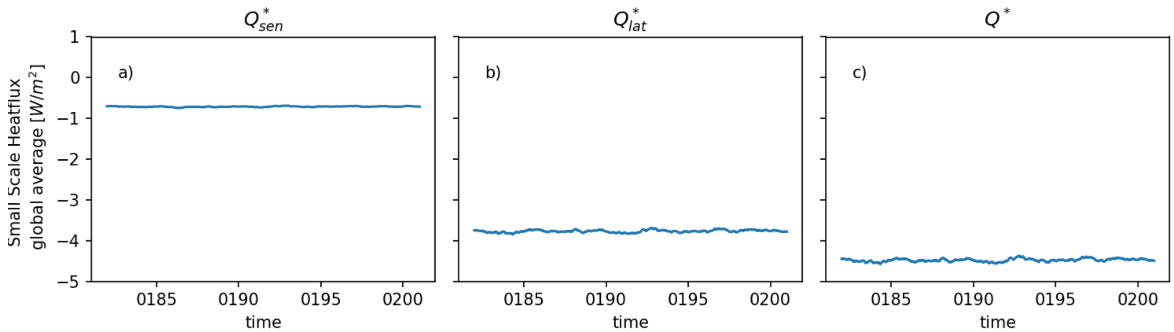

Figure 9: Global average small scale flux for CM2.6 and the ecmwf algorithm for sensible heatflux (a), latent heatflux (b), and combined turbulent heatflux (c). Each timeseries has a 360 day running mean applied to highlight interannual variability.

4.4 Main results seperated into latent and sensible heatflux

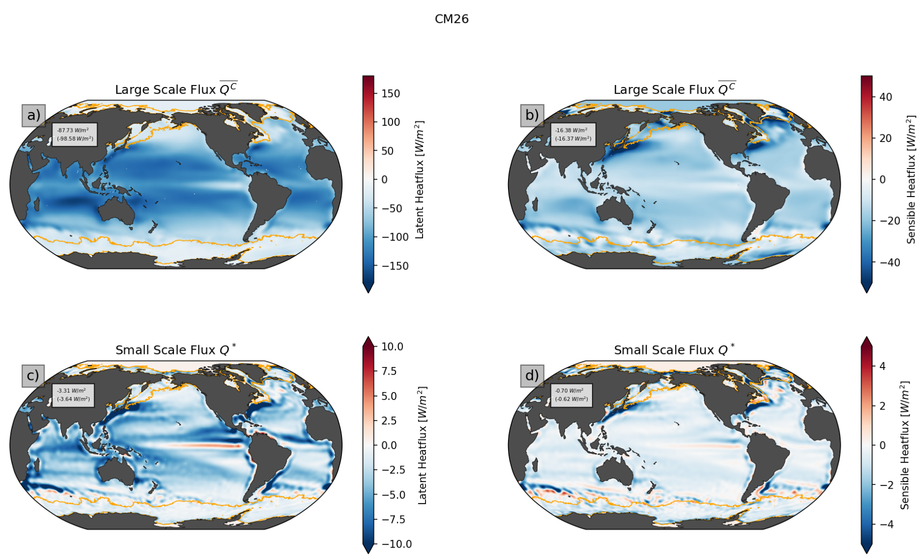

Figure 10: Columns as in Figure 2 in the main text, but shown for latent (left column) and sensible (right column) separately. Maps show averages of each term over 20 years of the CM2.6 simulation. Orange lines indicate the maximum extent of sea ice. Numbers shown in the top left of map panels indicate global averaged values for all available values and only ice free locations in parentheses. For details on treamtment of sea ice and temporal averaging see Temporal averaging and areas covered in sea ice.

Figure 10 shows the results for large scale and small scale flux separated into both individual components. The latent heat flux dominates the amplitude of the turbulent heat flux in most regions of the ocean. We further concluded that within each component individually the influence of small scales is to reinforce the large scale patterns (Figure 10). We also find that results from the second simulation also show qualitatively similar results (not shown). Future work that aims to implement a parametrization of the smale scale flux might have to consider both components individually, but for the purpose of this study we chose to present results for latent and sensible heatflux combined.